Dielectric and impedance spectroscopic studies of three phase graphene/titania/poly(vinyl alcohol) nanocomposite films

Saira Ishaq[a,b], Farah Kanwal[a,*], Shahid Atiq[c], Mahmoud Moussa[b], Umar Azhar[b], Iffrah Gul[d], Dusan Losic[b,*]

[a] Institute of Chemistry, University of the Punjab, Lahore 54590, Pakistan
[b] School of Chemical Engineering, The University of Adelaide, Adelaide 5005, SA, Australia
[c] Centre of Excellence in Solid State Physics, University of the Punjab, Lahore 54590, Pakistan
[d] Department of Electrical, Electronics and Telecom Engineering, University of Engineering and Technology (KSK Campus), Lahore 39020, Pakistan

ARTICLE INFO

ABSTRACT

Flexible dielectric polymer composites with high dielectric permittivity and low dielectric loss have many applications in different areas of electronic industry. In this paper, we propose synthesis of flexible dielectric materials with efficient dielectric properties. We increased dielectric efficiency of poly(vinyl alcohol) by reinforcement of conducting graphene and rutile titania fillers in different weight fractions. The superiority of this method is that synthesized three phase graphene/titania/poly(vinyl alcohol) nanocomposite films have high dielectric permittivity, low dielectric loss and are flexible. Our results show that graphene/titania/poly(vinyl alcohol) with weight/weight fraction of 3:20:100 bears dielectric permittivity of 330 at 20 Hz that is about 36 times larger than that of neat PVA at same frequency. At this frequency above mentioned graphene/titania/poly (vinyl alcohol) nanocomposite has loss tangent of 4.39 acceptable for dielectrics in embedded capacitors and AC conductivity of 1.6×10^{-6} Sm^{-1} that is much greater than that of neat PVA i.e; 6.5×10^{-9} Sm^{-1}. Complex impedance spectroscopy, complex electric modulus and Cole-Cole plots of synthesized graphene/titania/poly (vinyl alcohol) nanocomposite films further confirm its better capacitive performance.

Introduction

Materials possessing efficient dielectric properties are desired for a number of applications in different energy devices such as capacitors, transistors and humidity sensors [1–3]. Use of passive components reinforced in organic substrates is preferred over use of individual passive components. Such embedded composites have advantages of reduced size, light weight, low cost, better performance and increased reliability [4]. However selection of materials is of immense importance for miniaturization of embedded capacitors. Materials used for miniaturization of embedded capacitors must satisfy properties like ease of fabrication, mechanical stability, flexibility, fairly good electrical properties, high dielectric permittivity (ε'), low dielectric loss (ε''), low leakage current, high breakdown strength and high energy density [4,5]. Solely no material can own all desired characteristics; thus combining different materials of needed properties usually results in far more efficient materials.

Although polymers have low ε', rather they have advantages of flexibility, low density, low cost and easy processing [6]. ε' of polymers

can be grown by addition of high dielectric ceramics in it [7]. Sugumaran et al., synthesized titania/polyvinyl alcohol (TiO$_2$/PVA) and titania/poly(methyl methacrylate) (TiO$_2$/PMMA) nanocomposite films having ε' of 24.6 and 26.8, respectively at 1 kHz and low ε'' of 0.1–1.0 and 0.1–0.8, respectively at the same frequency [8]. Another composite was reported by Yu et al. They synthesized barium titanate nanotubes/polyvinylidene fluoride (BTNTs/PVDF possessing ε' of 47.05 with low ε'' of less than 0.1 [9]. Another strategy was to use conducting fillers in polymer matrix to improve dielectric properties of polymers [10]. He at al., synthesized a nanocomposite of PVDF with exfoliated graphite nanoplates exhibiting a very high ε' of 4.5×10^7 at 1000 Hz. However, ε'' of composite was also very high i.e; 229, thus limiting its merits over its demerits [11]. In another report, Kar at al., synthesized a nanocomposite of PVDF with exfoliated graphite submicron platelets exhibiting ε' of 33 at 100 Hz. However, tanδ of composite was also low i.e., less than 0.17 [12]. Yang et al; synthesized an excellent dielectric composite of ionic liquid coated carbon nanotubes (IL@CNT) with PVDF having ε' of 3323 and loss tangent (tanδ) of 12–13 [13]. Some researchers used both ceramic and conducting fillers within polymer
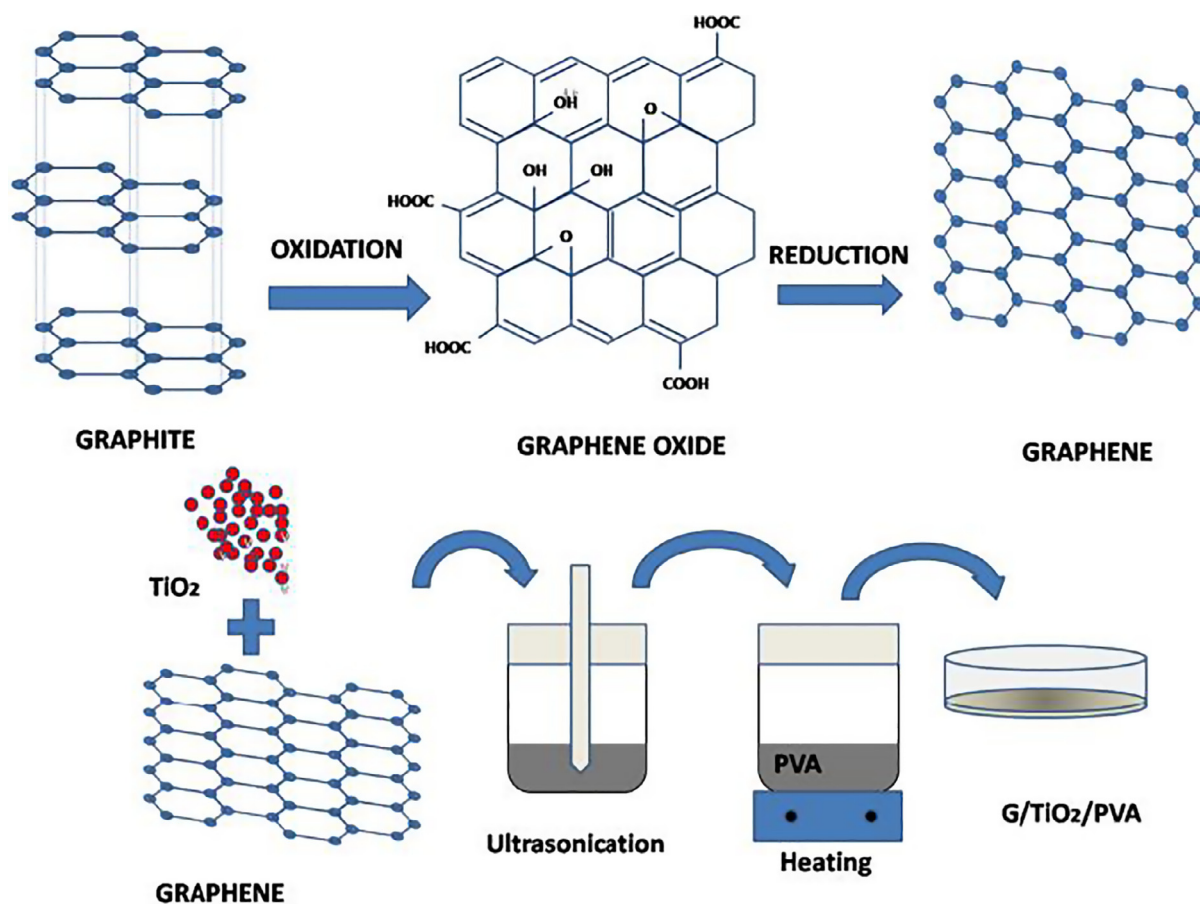

Fig. 1. Schematic diagram of the synthesis of G/TiO$_2$/PVA nanocomposite films.

matrix simultaneously. Li et al., increased ε′ of BaTiO$_3$/PVDF from 31.4 to 492 by addition of graphite but its ε″ was also raised from 0.026 to 49.1 at 1 kHz [14].

In this paper, we propose to demonstrate synthesis and characterization of efficient flexible dielectric polymeric materials with high ε′ and low ε″ by using a combination of ceramic and conducting fillers. For that purpose, we selected combination of three phase nanocomposite films containing graphene and TiO$_2$ as conducting and ceramic fillers, respectively in PVA. PVA as base polymer matrix was used due to its unique properties like water solubility, high capacitance and appropriate dielectric strength. Properties of PVA can be altered with incorporation of fillers which may also act as dopant [15]. TiO$_2$ in rutile phase was selected as ceramic filler because of its high ε′ of about 114 at room temperature (RT) [16]. But it has limitations like lack of mechanical stability [17]. If conducting filler is used along with ceramic filler, it can further surpass ε′ of the polymer. To address these limitations, we selected graphene due to its conducting nature, mechanical strength, ease of availability and feasible synthetic methods [18,19] and also providing high ε′ and low ε″. Schematic of synthesis of ternary G/TiO$_2$/PVA nanocomposite films is shown in Fig. 1. Dielectric efficiency of synthesized graphene/titania/poly(vinyl alcohol) (G/TiO$_2$/PVA) nanocomposite films was examined and discussed by calculating their ε′, tanδ, AC conductivity (σ$_{ac}$) and complex electric modulus (M*). Further complex impedance (Z*) of PVA and synthesized G/TiO$_2$/PVA nanocomposite films was measured and explained. Cole-Cole or Nyquist plot of PVA and G/TiO$_2$/PVA nanocomposite films were plotted to explicit their electrochemical performance. Synthesized material presented in this work has potential to be used as dielectric in embedded capacitors.

Experimental

Materials

Commercial natural graphite rocks (Uley, Eyre Peninsula, South Australia, Australia) were supplied from an Australian mining site. Sulfuric acid (98% H$_2$SO$_4$, Chem-Supply), hydrochloric acid (35% HCl, Chem-Supply), phosphoric acid (85% H$_3$PO$_4$, Chem-Supply), potassium permanganate (97% KMnO$_4$, Sigma-Aldrich), hydrogen peroxide (30% H$_2$O$_2$, Chem-Supply), titanium(IV) oxide (TiO$_2$, rutile, 99.98% trace metal basis, Aldrich) and poly(vinyl alcohol) (99.0–99.8% PVA, Sigma-Aldrich) were of analytical grade and were used without further treatment. High-purity milli-Q water (18.2 MΩcm at 25 °C, pH of 5.6) was used throughout the experiments.

Synthesis of G/TiO$_2$/PVA nanocomposite films

Graphene oxide (GO) was synthesized by an improved method [20]. GO was reduced to graphene by using hydrazine hydrate as reducing agent [21]. Ternary G/TiO$_2$/PVA nanocomposite was synthesized by solution mixing technique. Firstly, measured weight/weight (w/w) fractions of graphene and TiO$_2$ were dispersed in 10 mL of high-purity milli-Q water by ultrasonication. In the meanwhile, 1 g of PVA was dissolved in 20 mL of milli-Q water at 80 °C. After PVA was completely dissolved, solution of graphene/titania (G/TiO$_2$) was vigorously mixed in it at 80 °C till completely dissolved. The mixture was casted on petri dish, oven dried at 70 °C for few hours to completely remove moisture leaving behind G/TiO$_2$/PVA nanocomposite film.

Different G/TiO$_2$/PVA nanocomposites films of uniform thickness were casted by following the above described method with different w/w fraction of graphene, while keeping concentration of TiO$_2$ and PVA

Table 1
Sample codes with weight fraction of components of nanocomposite films.

Sample code	w/w fraction of G:TiO$_2$:PVA
Neat PVA	0:0:100
GTP-I	1:10:100
GTP-II	2:10:100
GTP-III	3:10:100
GTP-IV	4:10:100
GTP-V	3:15:100
GTP-VI	3:20:100
GTP-VII	3:25:100

constant. After dielectric characterization suitable weight fraction of graphene in G/TiO$_2$/PVA nanocomposite film with high ε′ and low tanδ was selected and further samples were synthesized by varying concentration of TiO$_2$ while keeping concentration of graphene and PVA constant. Schematic illustration of the synthesis of G/TiO$_2$/PVA nanocomposite films is given in Fig. 1. Table 1 shows w/w of all components of G/TiO$_2$/PVA nanocomposite films with their codes.

Characterization

Morphology of neat PVA and ternary G/TiO$_2$/PVA nanocomposite films was depicted by field emission scanning electron microscopy (FESEM, Quanta 450, FEI, USA). Structural studies were carried out by using X-ray diffraction (XRD, 600 Miniflex, Rigaco, Japan) and Raman spectroscopy (LabRam HR Evolution, Horiba jvon Yvon Technology, Japan). Fourier transform infrared (FTIR) spectroscopy (Nicolet 6700 Thermo Fisher) in range 400–4000 cm^{-1} was carried out to locate the functional groups. Thermal stability was studied by using a thermal gravimetric analyzer (TGA, Q500, TA Instruments, USA) under air where the samples were heated from room temperature to 900 °C at a heating rate of 10 °Cmin.$^{-1}$ Dielectric and impedance characterization of the synthesized G/TiO$_2$/PVA nanocomposite films were carried out using precision impedance analyzer (Wayer Kerr, 6500B) between 20 Hz and 2 MHz by placing sample films between copper electrodes at RT.

Results and discussion

Characterization of G/TiO$_2$/PVA nanocomposite films

Morphology of the synthesized G/TiO$_2$/PVA nanocomposite films was revealed by FESEM images shown in Fig. 2. Both graphene and TiO$_2$ nanoparticles are well dispersed in the PVA matrix. FESEM images in Fig. 2a–f depict that graphene sheets are not well aligned rather they are segregated due to TiO$_2$ nanoparticles and PVA matrix. Segregation of graphene sheets become more prominent with increasing TiO$_2$ fraction and are maximum in GTP-VII as shown in Fig. 2g. TiO$_2$ nanoparticles are dispersed on graphene sheets as well as are embedded in polymer matrix. It is evident from Fig. 2e–g that with increasing TiO$_2$ contents, its nanoparticles start to form large aggregates. Aggregations are more prominent in GTP-VII with maximum TiO$_2$ fraction as shown in Fig. 2g.

Fig. 3 shows XRD patterns of neat PVA and G/TiO$_2$/PVA nanocomposite films. A broad peak at 19.3° and a small peak at 29.4° are characteristic peaks of PVA [22]. Peaks for rutile phase of TiO$_2$ are present at 27.4° (1 1 0), 36.1° (1 0 1), 41.2° (1 1 1), 44.0° (2 1 0) and 56.5° (2 2 0) in accordance with JCPDS card no. 77–0441 [23]. However, in all the G/TiO$_2$/PVA nanocomposites, a very weak peak for graphene at 25.4° appears showing that graphene is fully exfoliated and well dispersed in PVA matrix [22,24]. With increasing w/w fraction of graphene and TiO$_2$ fillers, intensity of characteristic peak of PVA at 19.3° (1 0 1) is decreased suggesting that fillers and PVA are interacting
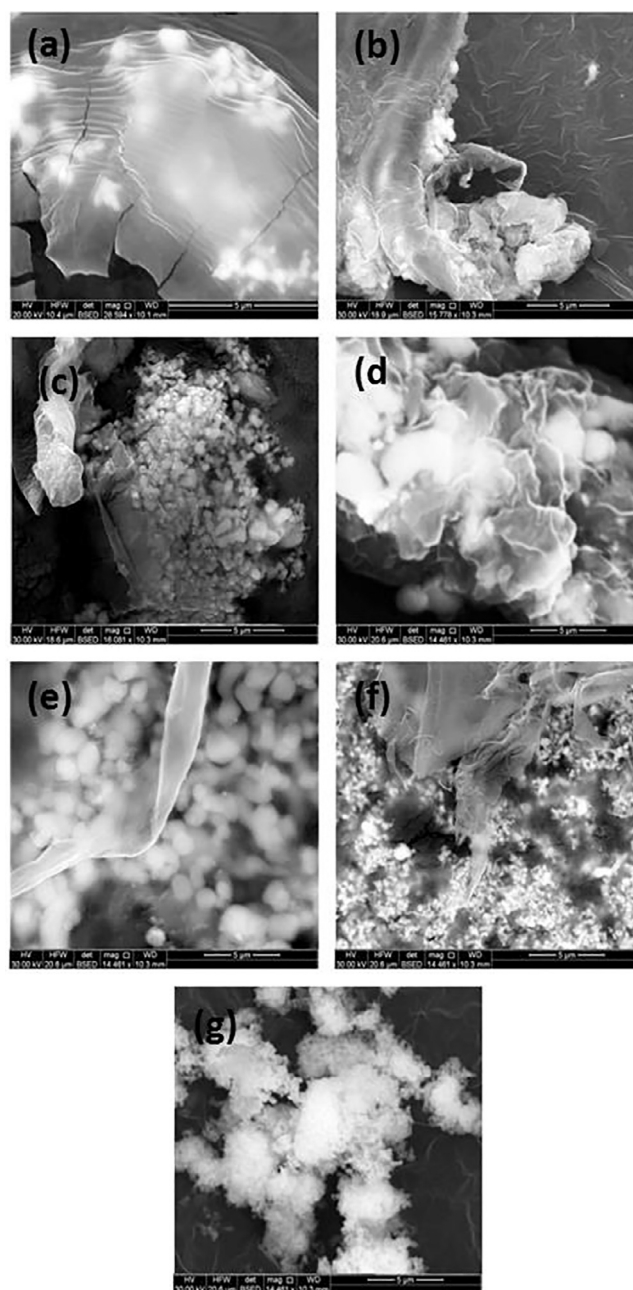

Fig. 2. FESEM images of G/TiO$_2$/PVA nanocomposites films (a) GTP-I (b) GTP-II (c) GTP-III (d) GTP-IV (e) GTP-V (f) GTP-VI (g) GTP-VII.

with each other. Broadening of peak suggests that crystalline structure of PVA is masked due to fillers [25].

Raman spectra of neat PVA and ternary G/TiO$_2$/PVA nanocomposite films of two samples i.e; GTP-III and GTP-VI shown in Fig. 4 have typical peaks of PVA film at 856 cm^{-1}, 910 cm^{-1}, 1013 cm^{-1}, 1148 cm^{-1}, 1221 cm^{-1}, 1335 cm^{-1}, 1442 cm^{-1} and 2916 cm^{-1} [26]. Weak peak at 445 cm^{-1} with small shoulder at 610 cm^{-1} belongs to rutile phase of TiO$_2$ [27]. Sharp peaks at 1334 cm^{-1} and 1592 cm^{-1} correspond to D and G bands of graphene, respectively [28].

Fig. 5 shows FTIR spectra of neat PVA and G/TiO$_2$/PVA nanocomposite films. In spectrum of pure PVA, broad peak in range of 3000–3600 cm^{-1} is attributed to stretching vibration of hydroxyl groups (–OH) in PVA. Peaks at 2951 cm^{-1} and 1000–1200 cm^{-1} confirm the presence of functional groups –CH$_2$ and C–O functional groups, respectively. However, peaks for –OH are shifted to lower wavenumber showing that hydrogen bonds of PVA are broken due to incorporation
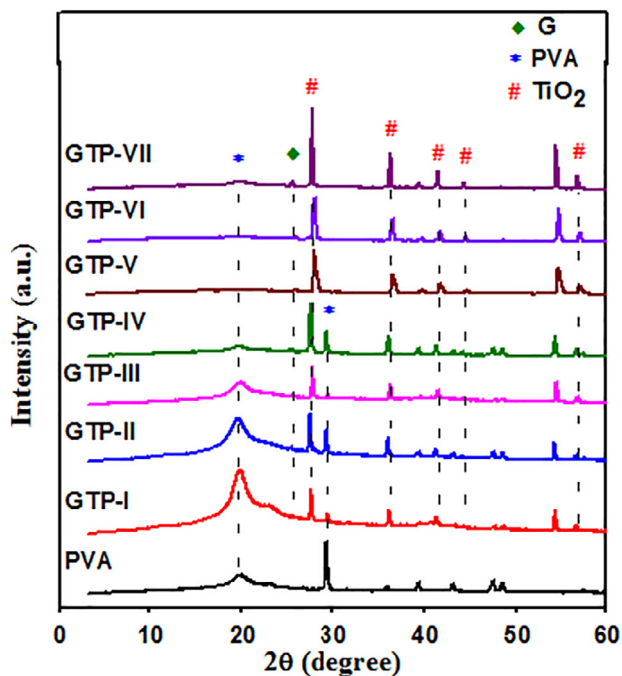
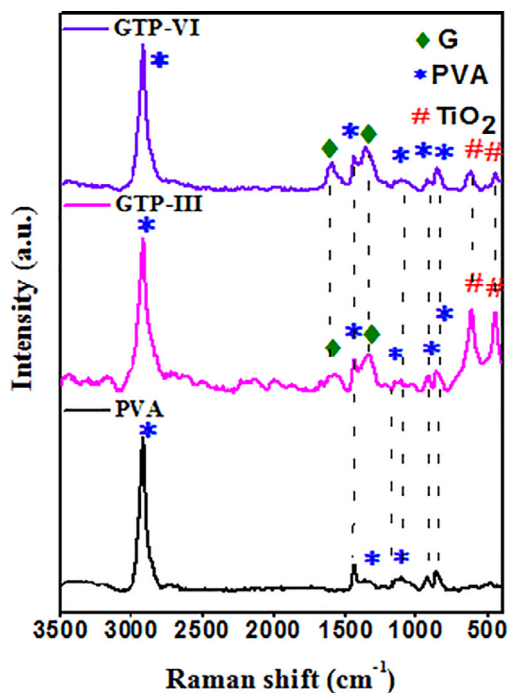**Fig. 3.** XRD patterns of neat PVA and G/TiO$_2$/PVA nanocomposites films.

Fig. 4. Raman spectra of neat PVA, GTP-III and GTP-VI nanocomposite films.

Fig. 5. FTIR spectra of neat PVA and G/TiO$_2$/PVA nanocomposite films.

Fig. 6. TG curves of neat PVA and G/TiO$_2$/PVA nanocomposites films.

of fillers and new hydrogen bonds between PVA and graphene are formed, a phenomenon known as hydrogen bond reduction effect [29]. Peaks for rutile phase of TiO$_2$ are observed at 471 cm^{-1} indicating Ti–O–Ti stretching vibration [30].

TGA analysis of neat PVA, GTP-III and GTP-VII nanocomposite films was carried out in the temperature range of 30–900 °C at a scan rate of 10 °Cmin^{-1} to study their thermal stability. Weight loss of about 7% for both neat PVA and G/TiO$_2$/PVA nanocomposite films between 30 and 200 °C is attributed to removal of moisture as shown in Fig. 6. Further constant weight loss observed between 200 and 500 °C is due to degradation of PVA chain which is c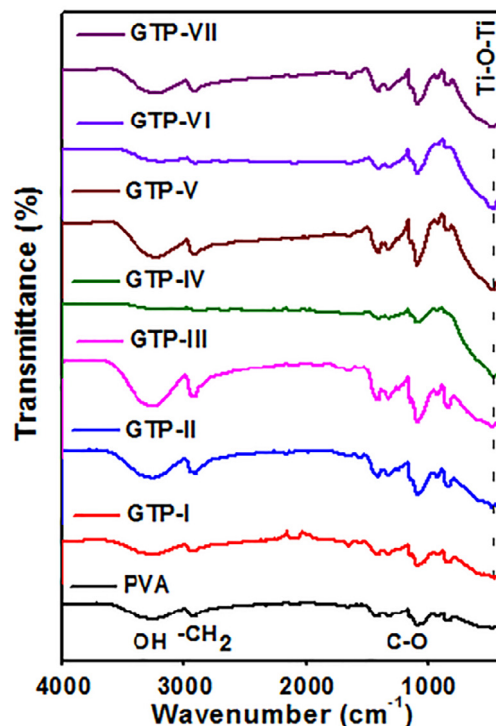ompletely degraded at 500 °C. While in GBP-IV and GBP-VII, after removal of moisture, further degradation starts at 225 and 245 °C, respectively showing that thermal stability is increased due to graphene and further by TiO$_2$. Maximum weight loss for GTP-IV and GTP-VII is 91 and 85%, respectively.

Dielectric and impedance studies of G/TiO$_2$/PVA nanocomposite films

Complex dielectric permittivity (ε^*) consists of real part of dielectric permittivity (ε') and imaginary part of dielectric permittivity (ε'') and is given by Eq. (1) [31]. ε' of PVA and G/TiO$_2$/PVA nanocomposite films was calculated by using Eq. (2).

$$\varepsilon^* = \varepsilon' - j\varepsilon'' \tag{1}$$

$$\varepsilon' = Ct/\varepsilon_o A \tag{2}$$

Here C is capacitance, t is thickness and A is the area of dielectric.
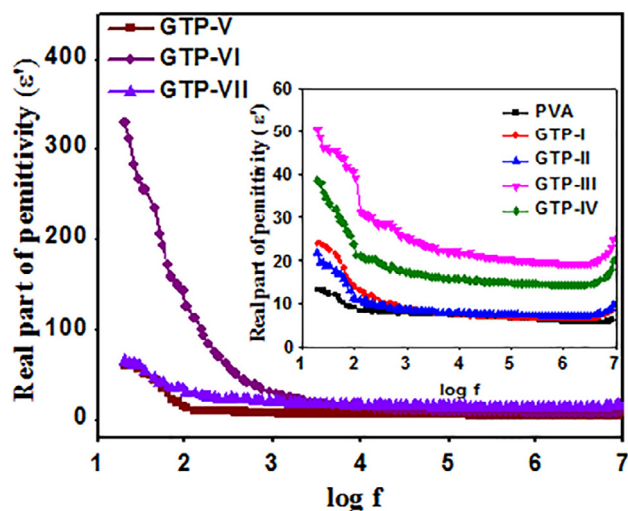
Fig. 7. Real part of permittivity (ε′) of neat PVA and G/TiO₂/PVA nanocomposites films.

While, ε_o is constant called vacuum permittivity bearing value of 8.85×10^{-12} F/m. ε′ of neat PVA and all synthesized G/TiO₂/PVA nanocomposite films was plotted as a function of frequency.

Fig. 7 shows that ε′ is high at low frequency, rapidly decreases with exceeding frequency and becomes constant at high frequency. In the low frequency region, electric field is slow, thus giving enough time to permanent and induced dipoles to align themselves well according to applied electric field. Thus, interfacial polarization (IP), also known as Maxwell Wagner Sillars (MWS) effect, is increased. At high frequency, decrease in ε′ is related to polarization relaxation phenomenon. At high frequency, alteration of electric field is quick due to which dipoles do not get sufficient time to align themselves; thus IP is relatively low, resulting in low ε′ [32]. At high frequency, ε′ is dominated by microcapacitor structure model i.e; becomes frequency independent and its value becomes constant. But still it is higher than that of neat PVA [11]. ε′ of nanocomposite elevates with increasing graphene weight fraction till GBP-III. GTP-III has ε′ of 50.6 at 20 Hz that is about 5.6 folds larger than that of neat PVA bearing ε′ of 9 at same frequency. Increased ε′ value is due to increase in both conductivity and IP. IP increases due to more free charges forming dipoles at interfaces of constituents. Both increased interfacial area and uniform distribution of nanofillers contribute to increase the IP [32,33]. When graphene is introduced in the nanocomposite, many microcapacitors are formed within the polymer matrix where graphene provides conducting pathways and act like electrodes, and PVA provides insulating media. With increasing graphene weight fraction number of microcapacitors in polymer matrix also multiplies to boost ε′ of the nanocomposite. However when graphene fraction is kept increasing, a stage reaches where graphene sheets are well connected to form an efficient conducting network as a result of which leakage current density exceeds and ε′ is depressed [34]. ε′ of

G/TiO₂/PVA nanocomposites further rises with increasing TiO₂ fraction, reaches a maximum value and then it starts decreasing after a certain w/w fraction of TiO₂. ε′ of GTP-VI was found as the largest among neat PVA and all G/TiO₂/PVA nanocomposite films as is evident from Fig. 7. GTP-VI exhibits ε′ of 330 that is 36 times larger than that of neat PVA film at 20 Hz. Increase in ε′ is attributed to high ε′ of TiO₂ filler instead of ε′ of polymer or graphene from GBP-V to GBP-VII. Increase in ε′ with increasing TiO₂ fraction is attributed to better network development for charge transport causing better conductivity. Efficiency of charge transport network increases with uniform distribution of TiO₂ in polymer [35,36]. Decrease in ε′ after further addition of TiO₂ in GBP-VII is attributed to formation of large aggregates as is evident by FESEM images in Fig. 2. Large TiO₂ aggregates can destroy charge transport network causing low ε′. ε′ values of neat PVA, GTP-III and GTP-VI at various frequencies are summarized in Table 2.

Energy dissipation (ε″) in dielectrics can be explained in form of tanδ which can be calculated by using Eq. (3) [31];

$$Tan\delta = \varepsilon''/\varepsilon' \qquad (3)$$

Tanδ of neat PVA and all G/TiO₂/PVA nanocomposite films decreases with rising frequency as shown in Fig. 8. With rise in graphene content tanδ also raises. It is due to reason that when electric field is applied to dielectric, graphene sheets can produce electric current and convert little part of electrical energy into thermal energy. Furthermore, graphene sheets are well connected to each other to form well aligned conducting pathways; thus causing increase in leakage current, ε″ and tanδ [34]. GTP-III has very low tanδ i.e; less than 1 at full frequency range i.e; between 20 and 2 MHz as shown in Fig. 8. However, tanδ further enhances with increasing TiO₂ fraction as shown Table 2. It is due to enhanced conductivity with increasing TiO₂ w/w fraction. These results are in accordance with previous findings [35,36]. But still tanδ is less than 5 at all frequencies which is desirable property for efficient embedded capacitors.

Comparative results of ε′ and tanδ of neat PVA and G/TiO₂/PVA nanocomposite films with different graphene and TiO₂ fractions at different frequencies are plotted in the form of graphs in Fig. 9a–d.

σ_{ac} of neat PVA and all G/TiO₂/PVA nanocomposite films was calculated by using Eq. (4) [37];

$$\sigma_{ac} = \varepsilon_o\varepsilon'\omega\tan\delta(\omega = 2\pi f) \qquad (4)$$

where, ω is angular frequency. σ_{ac} of neat PVA and all G/TiO₂/PVA nanocomposite films is shown in Fig. 10.

Results show σ_{ac} boosts with growing graphene w/w fraction. As more graphene is added more conducting pathways are developed causing increase in σ_{ac} of G/TiO₂/PVA nanocomposite. σ_{ac} further increases with increasing TiO₂ contents. Enhanced ε″ and tanδ may also be caused due to improved conductivity. Higher σ_{ac} of G/TiO₂/PVA nanocomposites with more TiO₂ fraction might be due to the presence of efficient network formation for charge transport. These results are in agreement with previously described reports [36]. σ_{ac} of GTP-VI is the largest among all G/TiO₂/PVA nanocomposite films. σ_{ac} of GTP-VI is 1.6×10^{-6} Scm^{-1} at 20 Hz which is many times larger than that of the

Table 2
Dielectric permittivity (ε′), loss tangent (tanδ) and AC conductivity (σ_{ac}) of neat PVA, GTP-III and GTP-VI.

Frequency (Hz)	Dielectric permittivity (ε′)			Loss tangent (tanδ)			AC conductivity (σ_{ac}) (Sm^{-1})		
	PVA	GTP-III	GTP-VI	PVA	GTP-III	GTP-VI	PVA	GTP-III	GTP-VI
20	13.3	50.6	330	0.7	2.1	3.8	7.2×10^{-9}	1.2×10^{-7}	1.7×10^{-6}
40	12.2	45	234	0.6	1.6	3.7	6.2×10^{-8}	1.6×10^{-7}	2.2×10^{-6}
100	9.1	39	126	0.1	0.47	3.3	6.8×10^{-9}	1.2×10^{-7}	2.8×10^{-6}
10^3	8.0	24.6	29.1	0.03	0.19	2.08	1×10^{-8}	2.6×10^{-7}	3.8×10^{-6}
10^4	7.4	21.7	13.1	0.05	0.08	0.72	2.0×10^{-7}	1×10^{-6}	6.5×10^{-6}
10^5	6.8	20.2	9.1	0.07	0.04	0.02	2.6×10^{-6}	4.6×10^{-6}	1.5×10^{-5}
10^6	6	19.3	7.5	0.08	0.03	0.11	2.9×10^{-5}	3.6×10^{-5}	5.7×10^{-5}
2×10^6	5.8	19.2	7.2	0.08	0.03	0.10	5.6×10^{-5}	7.0×10^{-5}	9.8×10^{-5}

Fig. 8. Loss tangent (tanδ) of neat PVA and G/TiO$_2$/PVA nanocomposites films.
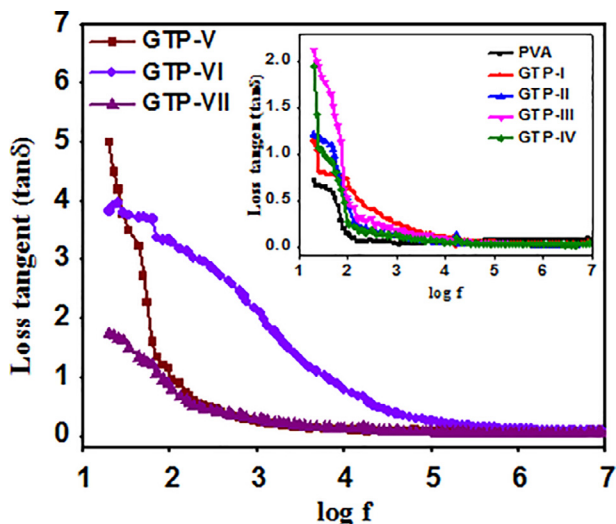
Fig. 10. AC conductivity (σ$_{a.c}$) of neat PVA and G/TiO$_2$/PVA nanocomposites films.

neat PVA possessing σ$_{ac}$ of 6.5×10^{-9} Scm^{-1} at the same frequency. σ$_{ac}$ of the neat PVA, GTP-III and GTP-VI are summarized in Table 2.

Complex impedance spectroscopy (CIS) was carried out to study conduction mechanism in neat PVA and G/TiO$_2$/PVA nanocomposite films. Complex impedance can be calculated from Eq. (5) [31];

$$Z^* = Z' + jZ'' = 1/j\omega C_o\varepsilon^* \tag{5}$$

Where, Z^*, Z', Z'', C_o represent complex impedance, real part of impedance, imaginary part of impedance and free space capacitance. While $j = (-1)^{1/2}$.

Figs. 11 and 12 show real and imaginary parts of impedance of the neat PVA and G/TiO$_2$/PVA nanocomposite films, respectively plotted against frequency. It is clear that both Z′ (resistance) and Z″ (reactance)
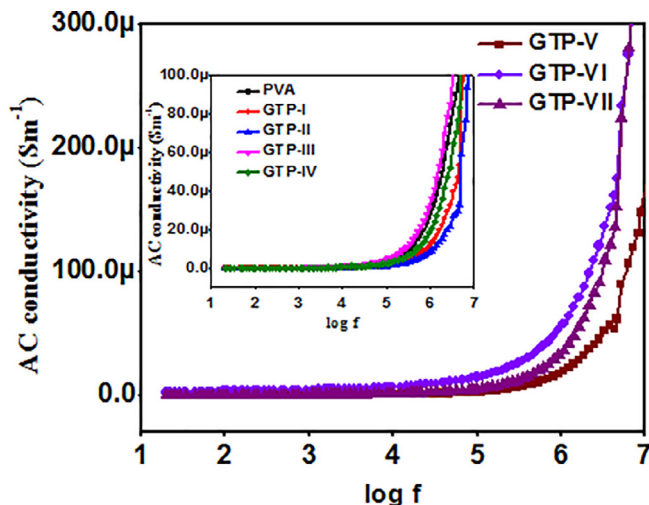
decrease with rise in frequency and become constant at high frequency well in accordance with previous reports [37]. Availability of more free space charges at high frequency is responsible for increased conduction [38]. Among all samples, GTP-VI has the lowest Z′, the highest σ$_{ac}$, and maximum ε′ among all synthesized nanocomposite films.

The dielectric modulus formalism is used to study the electrical transport within the dielectrics. Complex electric modulus (M*) was calculated by using Eq. (6) [31];

$$M^* = M' + jM'' = 1/\varepsilon^* \tag{6}$$

Where, M′ and M″ are real and imaginary part of electric modulus, respectively. M′ and M″ can be calculated by using Eqs. (7) and (8), respectively [31];
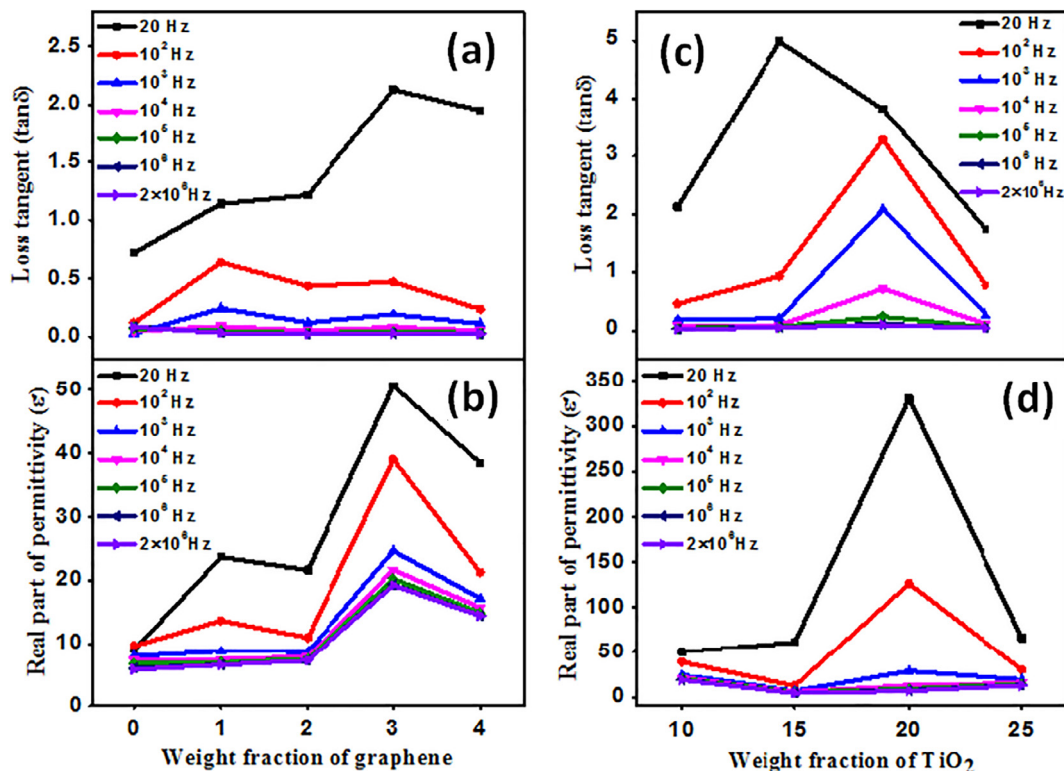

Fig. 9. (a) Loss tangent (tanδ) (b) Real part of permittivity of neat PVA and G/TiO$_2$/PVA nanocomposites films with different graphene fraction (c) Loss tangent (tanδ) (d) Real part of permittivity of neat PVA and G/TiO$_2$/PVA nanocomposites films with different TiO$_2$ fraction.
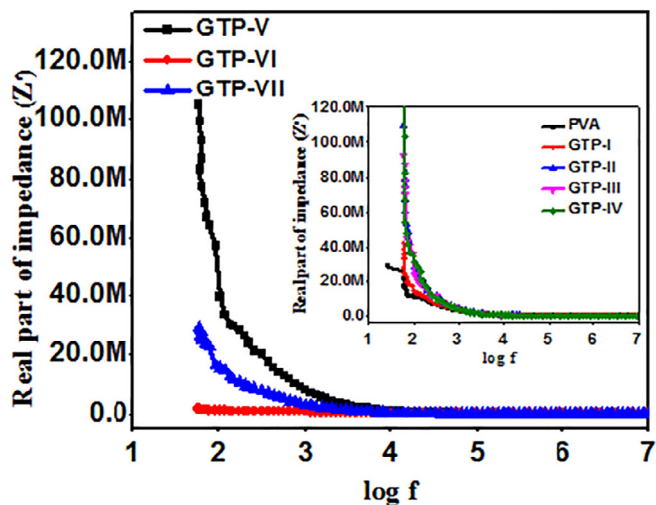
Fig. 11. Real part of impedance (Z′) of neat PVA and G/TiO$_2$/PVA nanocomposites films.
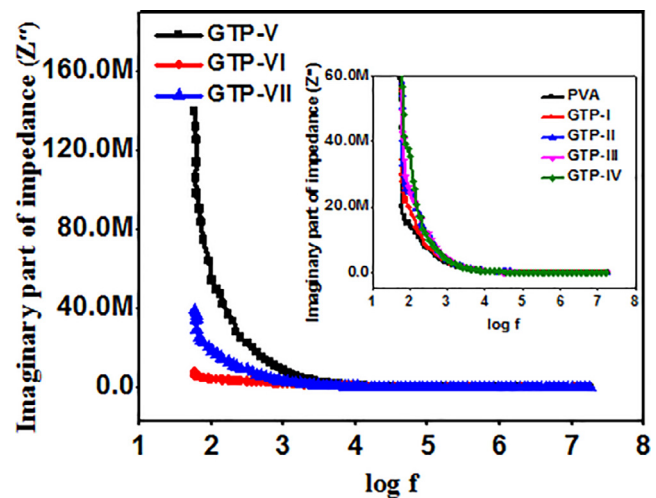

Fig. 12. Imaginary part of impedance (Z″) of neat PVA and G/TiO$_2$/PVA nanocomposites films.

$$M' = \varepsilon'/(\varepsilon'^2 + \varepsilon''^2) \tag{7}$$

$$M'' = \varepsilon''/(\varepsilon'^2 + \varepsilon''^2) \tag{8}$$

Fig. 13 illustrates the plots of M′ and M″ plotted against of frequency for neat PVA and all G/TiO$_2$/PVA nanocomposite films. As frequency is increased, M′ increases and reaches a maximum limit i.e; asymptotic value M$_\infty$ depicting that G/TiO$_2$/PVA nanocomposite films are capacitive in nature. This shows that relaxation processes exists over wide range of frequencies. Fig. 14 shows M″ plotted against frequency. It increases and reaches a maximum value M″max showing relaxation phenomenon. Then it starts decreasing with further increase in frequency [39]. It is because the charge carriers are mobile over long distance at low frequency below M″max as electric field alters slowly till M″max reaches. After reaching M″max when frequency increases, electric field changes rapidly so that charge carriers are mobile to short distance [40]. For GTP-IV, M″max shifts to low frequency region as compare to other G/TiO$_2$/PVA nanocomposite films with different graphene fraction. This shifting of M″max to lower frequency region shows increased conduction mechanism in GTP-IV which is due to more content of conducting graphene. As charge carriers are able to move over long and short distances at lower and higher frequencies, respectively, M″max shows transition of charge mobility from long range to
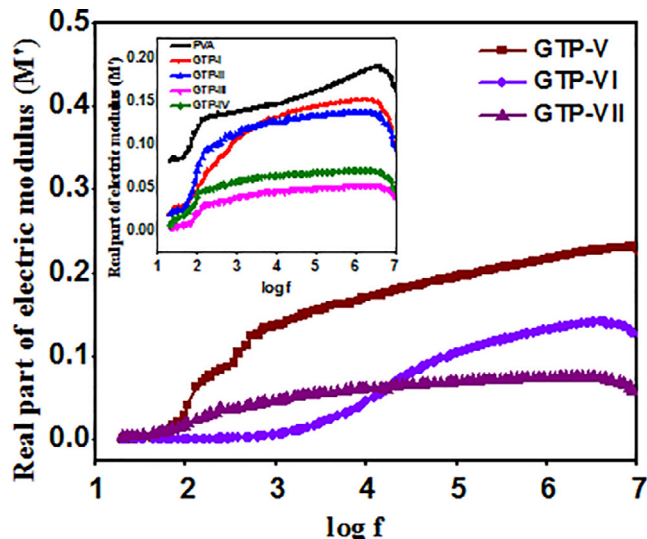

Fig. 13. Real part of electric modulus (M′) of neat PVA and G/TiO$_2$/PVA nanocomposites films.
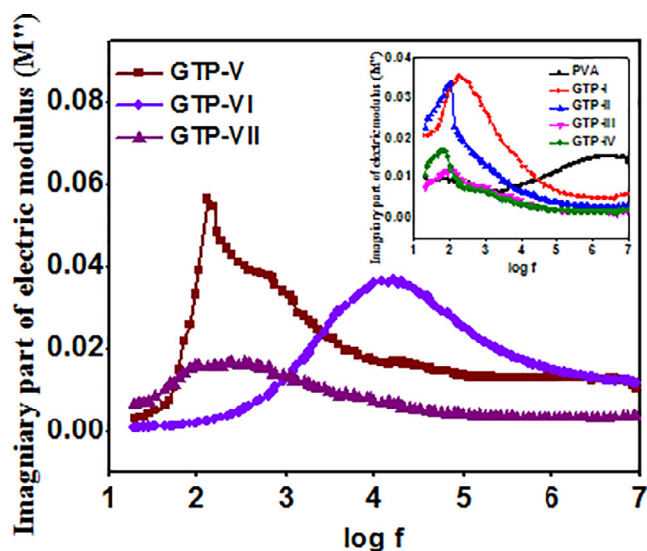

Fig. 14. Imaginary part of electric modulus (M″) of neat PVA and G/TiO$_2$/PVA nanocomposites films.
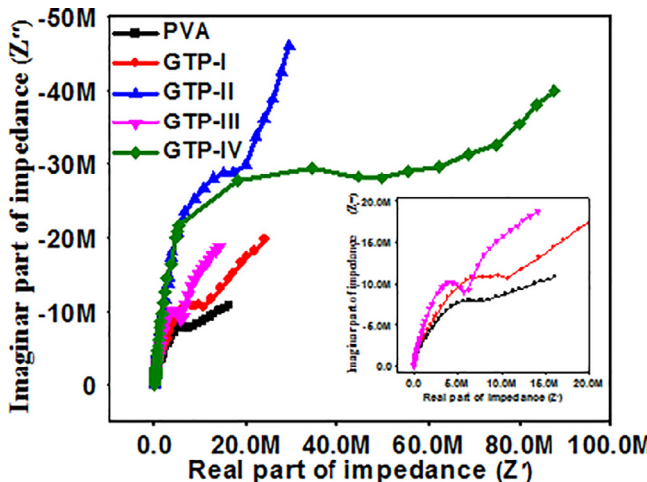

Fig. 15. Cole-Cole or Nyquist plots of neat PVA and G/TiO$_2$/PVA nanocomposites films with different graphene fraction.
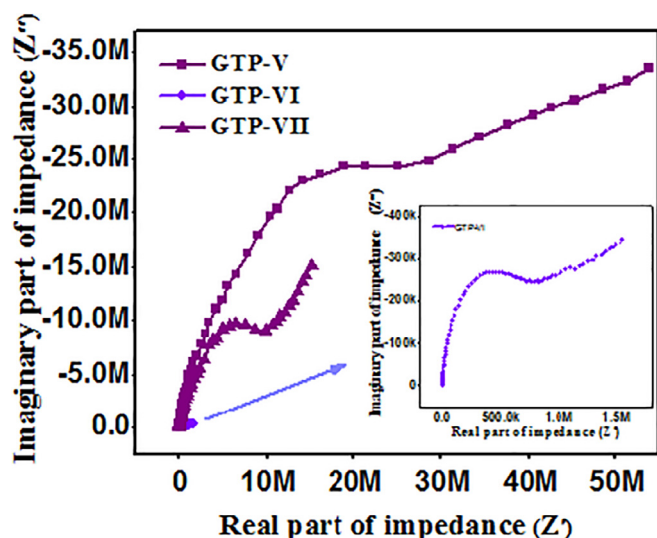
Fig. 16. Cole-Cole or Nyquist plots of neat PVA and G/TiO$_2$/PVA nano-composites films with different TiO$_2$ fraction.

short range [37].

Cole- Cole or Nyquist plot provides valuable information regarding electrical performance of materials in the form of semi circles. It is evident from Figs. 15 and 16 that neat PVA and all G/TiO$_2$/PVA nanocomposites show semi circles in their plots. However, diameter of semi circles varies in every nanocomposite film. Diameter of semi circle for GTP-III is the smallest among G/TiO$_2$/PVA nanocomposite films with different weight fraction of graphene i.e; from GTP-I– GTP-IV. It shows that GTP-III has more conductance than rest of nanocomposite films as is evident from their σ$_{ac}$ values in Fig. 10. When concentration of TiO$_2$ is changed from GTP-V to GTP-VII, diameter of semi circle is decreased as is shown in Fig. 16. GTP-VI has the smallest semi circle diameter showing that it has least resistance to flow of charges. It is also confirmed from σ$_{ac}$ of GTP-VI as shown in Fig. 10. All results are in accordance with each other. Increased ε′ of GTP-VI is attributed to its enhanced conductivity and decreased resistance.

Conclusion

Flexible dielectric graphene ceramic/PVA/composites with high ε′ and low tanδ were successfully synthesized by solution mixing technique. Dielectric efficiency of PVA was enhanced by reinforcement of conducting graphene and rutile TiO$_2$ fillers in different w/w. In first step, few G/TiO$_2$/PVA nanocomposite films were synthesized by varying weight fraction of graphene and keeping concentration of TiO$_2$ and PVA constant. After dielectric characterization, graphene concentration showing efficient dielectric properties was selected and new series of G/TiO$_2$/PVA nanocomposite films was synthesized by keeping concentration of graphene and PVA constant while varying concentration of TiO$_2$. Our results show that G/TiO$_2$/PVA with weight fraction of 3:20:100 has good dielectric efficiency being bearing ε′ of 330, tanδ of 4.39 and σ$_{ac}$ of 1.6×10^{-6} at 20 Hz. These results are much improved than that of neat PVA. M*, Z* and Cole-Cole plots further confirm that G/TiO$_2$/PVA nanocomposite film with w/w of 3:20:100 possess much better dielectric and impedance properties than neat PVA. Their practical application as dielectric in embedded capacitors is proposed.

Acknowledgements

References

[1] Cho S, Kim M, Lee JS, Jang J. Polypropylene/polyaniline nanofiber/reduced graphene oxide nanocomposite with enhanced electrical, dielectric, and ferroelectric properties for a high energy density capacitor. ACS Appl Mater Interfaces 2015;7(40):22301–14.
[2] Shin EY, Cho HJ, Jung S, Yang C, Noh YY. A high-k fluorinated P (VDF-TrFE)-g-PMMA gate dielectric for high-performance flexible field-effect transistors. Adv Funct Mater 2018;28(4):1704780.
[3] Huang X, Leng T, Georgiou T, Abraham J, Nair RR, Novoselov KS, et al. Graphene oxide dielectric permittivity at GHz and its applications for wireless humidity sensing. Sci Rep 2018;8(1):43.
[4] Lu J, Wong C. Recent advances in high-k nanocomposite materials for embedded capacitor applications. IEEE Trans Dielect El In 2008;15(5).
[5] Bai Y, Cheng Z-Y, Bharti V, Xu H, Zhang Q. High-dielectric-constant ceramic-powder polymer composites. Appl Phys Lett 2000;76(25):3804–6.
[6] Wang D, Dang Z-M. 12 – Processing of polymeric dielectrics for high energy density capacitors. In: Dang Z-M, editor. Dielectric Polymer Materials for High-Density Energy Storage. William Andrew Publishing; 2018. p. 429–46.
[7] Hdidar M, Chouikhi S, Fattoum A, Arous M, Kallel A. Influence of TiO$_2$ rutile doping on the thermal and dielectric properties of nanocomposite films based PVA. J Alloy Compd 2018;750:375–83.
[8] Sugumaran S, Bellan C. Transparent nano composite PVA–TiO$_2$ and PMMA–TiO$_2$ thin films: optical and dielectric properties. Optik 2014;125(18):5128–33.
[9] Pan Z, Yao L, Zhai J, Shen B, Wang H. Significantly improved dielectric properties and energy density of polymer nanocomposites via small loaded of BaTiO$_3$ nanotubes. Compos Sci Technol 2017;147:30–8.
[10] Ataur Rahman M, Chung G-S. Synthesis of PVDF-graphene nanocomposites and their properties. J Alloy Compd 2013;581:724–30.
[11] He F, Lau S, Chan HL, Fan J. High dielectric permittivity and low percolation threshold in nanocomposites based on poly (vinylidene fluoride) and exfoliated graphite nanoplates. Adv Mater 2009;21(6):710–5.
[12] Kar E, Bose N, Dutta B, Mukherjee N, Mukherjee S. Poly(vinylidene fluoride)/submicron graphite platelet composite: a smart, lightweight flexible material with significantly enhanced β polymorphism, dielectric and microwave shielding properties. Eur Polym J 2017;90:442–55.
[13] Yang J-H, Xiao Y-J, Yang C-J, Li S-T, Qi X-D, Wang Y. Multifunctional poly(vinylidene fluoride) nanocomposites via incorporation of ionic liquid coated carbon nanotubes. Eur Polym J 2018;98:375–83.
[14] Li Y, Tjong SC, Li R. Dielectric properties of binary polyvinylidene fluoride/barium titanate nanocomposites and their nanographite doped hybrids. Express Polym Lett. 2011;5(6).
[15] Subba Reddy CV, Han X, Zhu Q-Y, Mai L-Q, Chen W. Dielectric spectroscopy studies on (PVP + PVA) polyblend film. Microelectron Eng 2006;83(2):281–5.
[16] Roberts S. Dielectric constants and polarizabilities of ions in simple crystals and barium titanate. Phys Rev 1949;76(8):1215.
[17] Goh GK, Donthu SK, Pallathadka PK. Cracking and orientation of solution-deposited rutile TiO2 films. Chem Mater 2004;16(15):2857–61.
[18] Lee C, Wei X, Kysar JW, Hone J. Measurement of the elastic properties and intrinsic strength of monolayer graphene. Science 2008;321(5887):385–8.
[19] Balandin AA, Ghosh S, Bao W, Calizo I, Teweldebrhan D, Miao F, et al. Superior thermal conductivity of single-layer graphene. Nano Lett 2008;8(3):902–7.
[20] Marcano DC, Kosynkin DV, Berlin JM, Sinitskii A, Sun Z, Slesarev A, et al. Improved synthesis of graphene oxide. ACS Nano 2010;4(8):4806–14.
[21] Park S, An J, Potts JR, Velamakanni A, Murali S, Ruoff RS. Hydrazine-reduction of graphite-and graphene oxide. Carbon 2011;49(9):3019–23.
[22] Jan R, Habib A, Akram MA, Khan AN. Uniaxial drawing of graphene-PVA nanocomposites: improvement in mechanical characteristics via strain-induced exfoliation of graphene. Nanoscale Res Lett 2016;11(1):377.
[23] Wang C, Zhang X, Shao C, Zhang Y, Yang J, Sun P, et al. Rutile TiO$_2$ nanowires on anatase TiO$_2$ nanofibers: a branched heterostructured photocatalysts via interface-assisted fabrication approach. J Colloid Interface Sci 2011;363(1):157–64.
[24] Lei Z, Lu L, Zhao XS. The electrocapacitive properties of graphene oxide reduced by urea. Energy Environ Sci 2012;5(4):6391–9.
[25] Yang X, Li L, Shang S, Tao X-M. Synthesis and characterization of layer-aligned poly (vinyl alcohol)/graphene nanocomposites. polymer 2010;51(15):3431–5.
[26] Cooney T, Wang L, Sharma S, Gauldie R, Montana A. Raman spectral study of solid and dissolved poly (vinyl alcohol) and ethylene-vinyl alcohol copolymer. J Polym Sci, Part B: Polym Phys 1994;32(7):1163–74.
[27] Zhang W, He Y, Zhang M, Yin Z, Chen Q. Raman scattering study on anatase TiO$_2$ nanocrystals. J. Phys. D 2000;33(8):912.
[28] Yaqoob U, Uddin AI, Chung G-S. The effect of reduced graphene oxide on the dielectric and ferroelectric properties of PVDF–BaTiO$_3$ nanocomposites. RSC Adv 2016;6(36):30747–54.
[29] Bao C, Guo Y, Song L, Hu Y. Poly(vinyl alcohol) nanocomposites based on graphene and graphite oxide: a comparative investigation of property and mechanism. J Mater Chem 2011;21(36):13942–50.

[30] Djaoued Y, Badilescu S, Ashrit PV, Bersani D, Lottici PP, Robichaud J. Study of Anatase to Rutile Phase Transition in Nanocrystalline Titania Films. J Sol-Gel Sci Technol 2002;24(3):255–64.

[31] Li Y, Huang X, Hu Z, Jiang P, Li S, Tanaka T. Large dielectric constant and high thermal conductivity in poly(vinylidene fluoride)/barium titanate/silicon carbide three-phase nanocomposites. ACS Appl Mater Interfaces 2011;3(11):4396–403.

[32] Tantis I, Psarras G, Tasis D. Functionalized graphene–poly (vinyl alcohol) nano-composites: physical and dielectric properties. eXPRESS Polym Lett 2012;6(4).

[33] Kalini A, Gatos K, Karahaliou P, Georga S, Krontiras C, Psarras G. Probing the dielectric response of polyurethane/alumina nanocomposites. J Polym Sci, Part B: Polym Phys 2010;48(22):2346–54.

[34] Ping F, Lei W, Jintao Y, Feng C, Mingqiang Z. Graphene/poly(vinylidene fluoride) composites with high dielectric constant and low percolation threshold. Nanotechnology 2012;23(36):365702.

[35] Li J, Seok SI, Chu B, Dogan F, Zhang Q, Wang Q. Nanocomposites of ferroelectric polymers with TiO2 nanoparticles exhibiting significantly enhanced electrical

[36] Mo T-C, Wang H-W, Chen S-Y, Yeh Y-C. Synthesis and dielectric properties of polyaniline/titanium dioxide nanocomposites. Ceram Int 2008;34(7):1767–71.

[37] Amin M, Rafique HM, Yousaf M, Ramay SM, Atiq S. Structural and impedance spectroscopic analysis of Sr/Mn modified BiFeO3 multiferroics. J Mater Sci – Mater Electron 2016;27(10):11003–11.

[38] Atiq S, Majeed M, Ahmad A, Abbas SK, Saleem M, Riaz S, et al. Synthesis and investigation of structural, morphological, magnetic, dielectric and impedance spectroscopic characteristics of Ni-Zn ferrite nanoparticles. Ceram Int 2017;43(2):2486–94.

[39] Pradhan D, Samantaray B, Choudhary R, Thakur A. Complex impedance analysis of layered perovskite structure electroceramics—NaDyTiO₄. J Mater Sci 2005;40(20):5419–25.

[40] Singh G, Tiwari V. Effect of Zr concentration on conductivity behavior of (1–x) PMN-xPZ ceramic: an impedance spectroscopy analysis. J Appl Phys 2009;106(12):124104.

energy density. Adv Mater 2009;21(2):217–21.